ISSN 1068-3755, Surface Engineering and Applied Electrochemistry, 2016, Vol. 52, No. 4, pp. 334–341. © Allerton Press, Inc., 2016.

The Effect of Monomer and Clay Proportion on the Formation of Polypyrrole Clay Intercalated Nanocomposite[1]

R. Zidi*, I. Bekri-Abbes, and E. Srasra

Physical Chemistry Laboratory for Mineral Materials and Their Applications, National Center for Research in Materials Sciences (CNRSM), B.P.73–8020, Soliman-Tunisia

**e-mail: rabiizidi@gmail.com*

Received May 5, 2015; in final form, July 24, 2015

Abstract– In this study, intercalated polypyrrole/montmorillonite nanocomposite was synthesized by a facile and simple solution intercalation method. The method is based on the exchanging of pyrrole monomers with sodium interlayer cations followed by polymerization by adding ammonium persulfate as oxidant. To avoid the spontaneous polymerization of pyrrole outside the clay, the proportions of pyrrole to clay and that of monomer to oxidant were varied. Several techniques have been used to study the structure and conductivity of the obtained materials: Fourier transform infrared spectroscopy, X-ray diffraction, Energy-dispersive X-ray spectroscopy analysis, scanning electron microscopy, Brunaner–Emmet–Teller technique, impedance spectroscopy and ultraviolet–visible spectroscopy. It was shown that it is not necessary to subject clay to organophilation with quaternary alkylammonium or to ultrasonic activation, or to treat it thermally to form intercalated nanocomposite. By increasing the amount of clay to that pyrrole, an intercalated polypyrrole clay nanocomposite is formed. Theevidence of the intercalation of polypyrrole is deduced from the X-ray diffraction and the Brunaner–Emmet–Teller technique specific surface. Both the expansion of the basal interlayer distance to 14 Å and the decrease of the specific surface area from 78.2 for the clay to 48 $m^2 g^{-1}$ prove the formation of an intercalated structure. The conductivity has been measured using impedance spectroscopy. The *dc* conductivity was in the range of $2–10^{-3}$ S/cm.

Keywords: nanocomposite, microcomposite, polypyrrole, montmorillonite, intercalation, conductivity

DOI: 10.3103/S1068375516040141

INTRODUCTION

Polypyrrole (PPy) is the subject of numerous studies due to its good environmental stability and high electrical conductivity. This conductive polymer can be potentially used in batteries, supercapacitors,sensors, anhydrous electrorheological fluids, microwave shielding and corrosion control [1–3]. There are different approaches for preparation of PPy. These includes polymerization of pyrrole (py) in solution [4] or emulsion [5, 6], electropolymerization in the presence of inorganic materials [7], exposure of oxidant-adsorbed host material to py vapour [8] and grafting of PPy on the host material via functional groups on inorganic particles [9]. In general, PPy is brittle, insoluble and infusible, hence it is not possible to process it. Over the last decades, a great effort has been invested in both academic and industrial areas into enhancing its processing potential. In order to improve its properties, a number of PPy nanocomposites have been prepared [10–12]. The location of the PPy whether on the external surface of the clay crystal or inside the interlayer space has an important effect on the properties of theobtained material complex. When PPy is localized outside the clay interlayer it forms a conventional microcomposite material. However, when PPy chains are intercalated in interlayers of clay, PPys with an ordered chain structure and better properties can be obtained [13]. Biswas et al. have prepared Montmorillonite (Mt)/PPy through the polymerization of py with Mt containing iron redox sites [14]. From the X-ray diffraction (XRD) analyses, it was shown that PPy has not been intercalated into the Mt lamellale because of the spontaneous external polymerization of py. In order to obtain the intercalated structure, several attempts have been made in the literature based on the organo-modification of clay or on its mechanoche-mical or thermal treatment. Mravcakovà and colleagues have studied the effect of the organic modification of clay on the chemical and electrical properties of nanocomposite [15]. For the same reason, Goa and colleagues have proved that a step of ultrasonic and a decrease of the temperature to 0°C is necessary to ensure the formation of intercalated nanocomposite [16]. Letaief and colleagues have studied in detail the effect of the localization of iron cation and the amount of iron on the spontaneous polymerization of py out-

[1]The article is published in the original.

side or in the clay interlayer [16]. They have shown that the ions of iron localized in the clay interlayer induce the intercalation of PPy and thus an intercalated nanocomposite is obtained, however when iron is localized in the octahedral sheet of clay, the spontaneous polymerization of py outside the clay interlayer is more rapid than the diffusion to the interlayer. In the same context, Faguy and colleagues have used in situ the attenuated total reflectance Fourier transform infrared spectroscopy (ATR-FTIR) to follow the evolution (in real time) of the oxidative polymerization of py in Fe^{3+}-montmorillonite [18], which indicated that the overall process consists of three steps: pre-concentration, polymerization and py diffusion. This sequence indicates that the polymerization is only initiated after a certain amount of py is present in the medium and it lasts until the oxidation capacity has been exhausted.

From all these studies it follows that a spontaneous polymerization of py outside the clay interlayer can be avoided by increasing the proportion of clay to that of py. In this way, the pre-concentration of py is blocked and a non-spontaneous polymerization outside the clay is avoided. Thus a difference of the present study compared to those reported in literature is that we investigate the preparation of an intercalated PPy clay nanocomposite with high-amounts of clay. It is important to mention that the volume of ammonium persulfate is a major factor that determines whether there is the intercalation of PPy in the clay interlayer and the formation of nanomaterial or not.

EXPERIMENTAL

Py monomer (98%, Aldrich) was distilled under a reduced pressure. Ammonium persulfate (APS) ($(NH_4)_2\ S_2O_8$, oxidant) and hydrochloric acid were purchased from Aldrich and were used withoutfurther purification. Natural clay from Elfahs (North West of Tunisia) consists mainly of an interstratified illite-montmorillonite with minor kaolinite, quartz and calcite impurities. Purified clay was obtained by sedimentation, centrifugation and drying (method of Van Olphen (1963) [19]. The chemical composition of the montmorillonite was found to be as follows: 52.62% SiO_2, 3.09% MgO, 18.44% Al_2O_3, 1.12% K_2O, 0.52% CaO, 1.92% Na_2O, 3.52% Fe_2O_3 and 18.73% loss on ignition. The cation-exchange capacity (CEC) of the clay sample was 100 Meq per 100 g dry clay. Py/clay hybrid materials were prepared by dispersion of Mt in 50 mL of distilled water and by adding the py dispersed in water and stirred. The share of py varied from 0.25 CEC to 4 CEC of the clay. Py–montmorillonite hybrid materials were denoted as Mt-Py (*n*), where (*n*) indicated the ratio of py to the CEC of the clay. Mt/PPy nanocomposites were prepared by dispersing the Mt-Py (4) hybrid material in an aqueous solution, and then APS was added to the dispersion. The relative ratio of APS/py varied, with the mole ratio ranging from 0.25 to 4. The resultant black suspension was centrifuged with distilled water to remove the excess monomer and impurities. The procedure wasrepeated until the supernatant was colorless. The black slurry was allowed to dry in the ambient laboratory environment. The samples were denoted Mt/PPy(*R*), where (*R*) indicated molar ratio of APS to Py. The amount of py localized in the hybrid material has been deduced from py concentration released in the supernatant after purification of the nanocomposite determined using PERKIN ELMER (model LAMBDA 20) spectrophotometer.

The synthesized materials were examined by the X-ray diffraction through a Panalytical diffractometer using Cu radiation. The IR spectra were collected with a Nicolet spectrophotometer model 560 in a scanning range from 400 to 4000 cm^{-1}. The samples were prepared as KBr pellet. The electrical conductivity was measured for different samples prepared as pellets under a pressure of 10 Mg/cm^2 and coated on both sides with silver paint using a Hewlett Packard model 4192A impedance analyser in the 0.01 kHz–10 MHz frequency range. The conductivity of the samples was calculated from the impe-dance data, using the relation:

$$\sigma = \frac{1}{R' \times S}, \quad (1)$$

where *L* and *S* are the thickness and face area of the sample, respectively, and *R*' was derived from the low intersect of the high frequency semi-circle on a complex impedance plane with the Re (*Z*) axis.

The micro- and nanostructure of nanocomposites were identified by a Scanning Electronic Microscope (SEM) Zeiss Supra 35 (back-scattered electron mode) combined with an EDX LEO 1530, thus allowing the identification of the different elements.

The specific surface area and the total porevolume were measured by an automatic adsorption instrument (Autosorb I); the amount of py monomer intercalated was determined using UV-visible absorption spectra (at a PERKIN ELMER (LAMBDA 20) spectrophotometer).

RESULTS AND DISCUSSIONS

Characterization of Mt-Py Hybrid Materials

The aim of the present section is to study theinteraction of a py monomer with a high amount of clay containing redox sites and to visualize whether or not the octahedral structural iron has induced a spontaneous polymerization of py outside the clay interlayer.

Figure 1 shows the FTIR spectra of Mt, py and py/Mt hybrid materials for different proportions of py to CEC of Mt that varied from 0.25 to 4. The characteristic peaks for Mt were composed essentially of broad hydroxyl and silanol bands at 3200–3700 and 900–1200 cm^{-1}, respectively [20], the peaks at 518 and

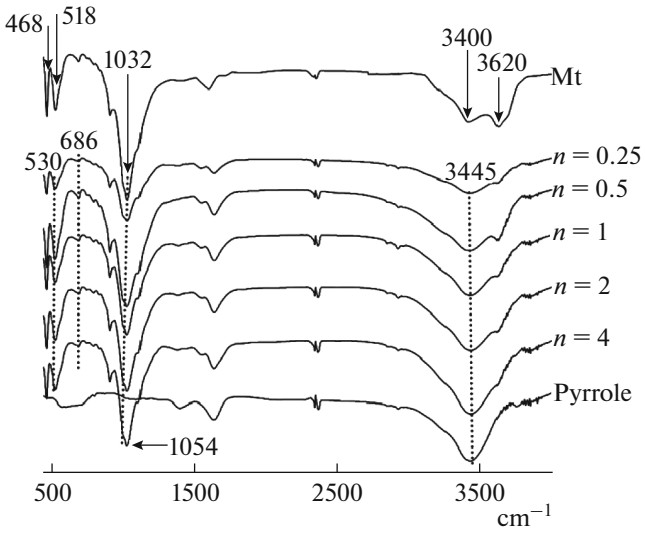

Fig. 1. FTIR spectra of Mt, Py and Mt-Py (*n*) hybrid materials for different proportions of py to CEC of Mt.

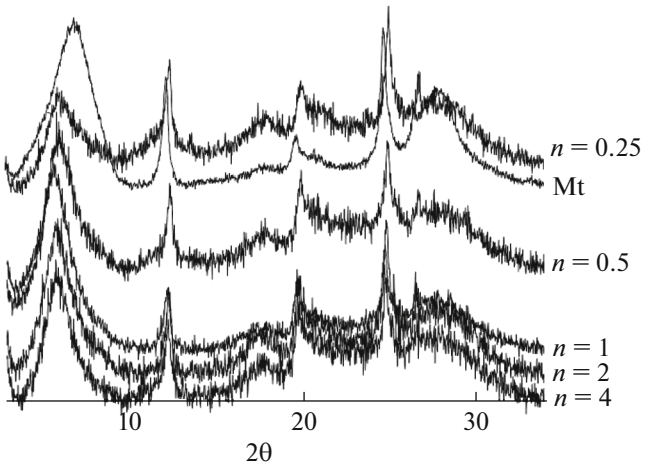

Fig. 2. XRD patterns of Mt and Mt-Py (*n*) hybrid materials for different proportions of py to CEC of Mt.

468 cm^{-1} corresponded to υ_{Si-O}, and δ_{Si-O} [21]. The identification of vibration modes of py had been assigned as in [22, 23]. The bands localized at 1512–1530 and 1418–1449 were assigned to $\upsilon_{C=C}$ symmetric and υC=N antisymmetric characteristic vibration modes of the py molecule [23, 24]. In order to evaluate the mode of interaction of py with the clay, it is necessary to study the Si–O stretching of the clay and the H–O–H bending region of H_2O; the position of the vibration of Si–O stretching was gradually shifting towards a higher frequency, this is supposed to be due to the Coulomb interaction between the nitrogen of the py layer and the partially negatively charged surface of the clay [25]. In addition, with the intercalation of py, the intensity of the band attributed to the H–O–H bending region of H_2O localized at 1610 cm^{-1} decrease because of the partial replacement of the H_2O interlayer by py molecules. Thus, it could be stated that the vibration peaks of py were presented in the FTIR spectra of different hybrid materials with a slight shift resulting from the interactions between the py functional groups and the clay functional groups. From the FTIR analysis, it can be concluded that the polymerization of py induced by the redox active structural iron clay did not take place. By decreasing the loading amount of py compared to clay, it became possible to stop the steps of pre-concentration and polymerization. These results indicate that, in a similar way to that observed by Faguy and colleagues [18], the polymerization is only initiated when the monomer concentration reaches a determined level.

Table 1. Py content and basal spacing of clay samples adsorbed to py for variable CEC

	Py content (mmol/100 g clay)	d_{001} (Å)
Mt	–	12.1
0.25	17.3	14.6
0.5	40.8	14.63
1	43	15.22
2	162.3	15.10
3	164	15.16
4	202	15.32
5	200	15.12

Using Table 1 and Fig. 2, it can be mentioned that for all materials, the d_{001} basal spacing has shif-ted toward higher values after adding of py, which has proved a successful intercalation of py within the clay layers**.** However the d_{001} changes its position depending on the molar ratio of py to interlayer sodium. Taking into account the thickness of the silicate layer (9.6 Å), a Δd_{001} value varying from 5 Å to 5.62 Å was obtained for these composites on adding py. The size of a py ring was calculated theoretically by the Complete Neglect of Differential Overlap method or by molecular simulation is about 0.4 nm [26, 27]. The Δd_{001} is compatible to an arrangement in a monolayer with the py rings extended parallel to the silicate layer. Considering this model and the total amount of py retained by the clay it could be admitted that for (*n*) corresponding to 0.25, 0.5 and 1, the amount of retained py by clay ranged from 17 to 43 mmol/100 g of the clay thus py has been intercalated in the clay galleries with a monolayer arrangement located perpendicular to the clay layers [28]. For (*n*) corresponding to 5, py retained in the clay increases to reach a value of 200 mmol/100 g of the clay. The supplementary quantity of py is thought to be adsorbed on the clay surface.

Characterization of Mt-PPy Nanocomposite

To induce polymerization of intercalated py, APS has been used. Similar to the polymerization mechanism of most conducting polymers, py is first oxidised to a polymer and then to a cationic form of PPy doped with anions, with a positive charge on, at most, every 3–4 py units [29]. Scheme 1 demonstrates the polyme-rization process of py; in theory an APS/py ratio equal to 1 is required for a complete oxidation of py to a fully doped polymeric form:

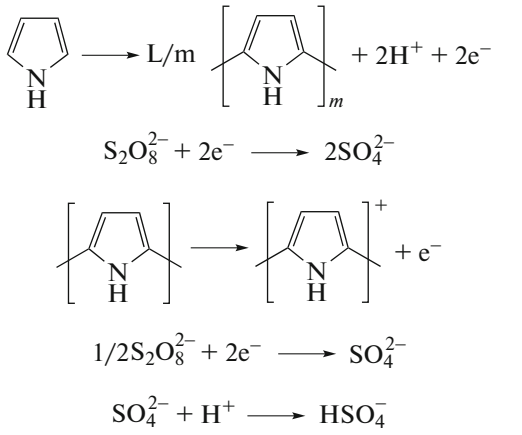

Scheme 1. Polymerization of py.

Infrared spectra of different samples are given in Fig. 3. FTIR spectra can be used to investigate the presence of PPy and its interactions with the Mt host vibrations [25–30]. The band at 1550 cm^{-1} is assigned to the py ring, i.e., the combination of C=C and C–C stretching vibrations. The peak at 1455 cm^{-1} is associated to the C–N stretching vibration. The peaks at 1309, 1185, and 920 cm^{-1} are attributed to the in-plain vibrations of C–H. A strong broad band at around 3435 cm^{-1} corresponds to the N–H stretching vibration for PPy. The peaks at 780 and 670 cm^{-1} are attributed to the out-of-the plane deformation of the C–H bond [22]. For the PPy-Mt nanocomposite, the spectrum clearly exhibits the characteristic absorption peaks associa-ted to PPy chains (Fig. 3*e*) and Mt (Fig. 3*a*) with peak shifts indicating the presence of an interaction between Mt and PPy. With an increase of the amount of APS ($R = 4$), in Fig. 3b it can be seen that there appeared a band around 1700 cm^{-1} due to the overoxidation of PPy and the disappearance of the peaks localized at 1309, 1455 and 1550 cm^{-1}. The same observation has been made in [17] when testing the adsorption of py in the clay with a very high content of structural iron.

In Fig. 4, the XRD diffractograms of PPy/Mt nanocomposites are presented for different molar ratio of APS to py (R). A d_{001} basal spacing shift, depending on the R value, can be observed after the adding of an oxidant, and this shift proves that the structure has been changed. The basal spacing d_{001} is localized at

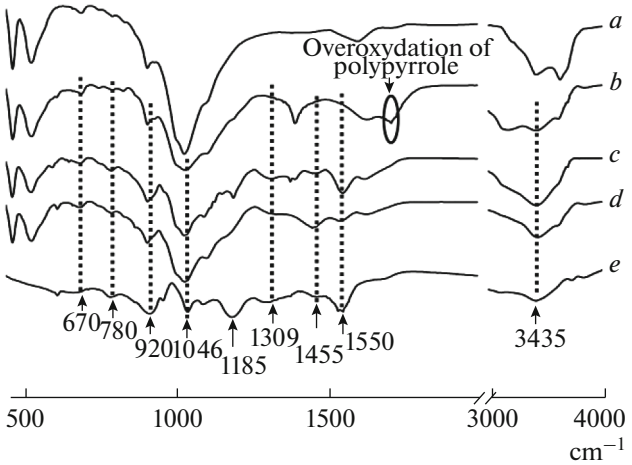

Fig. 3. FTIR spectra of: (*a*) Mt; (*b*) Mt/PPy ($R = 4$); (*c*) Mt/PPy ($R = 1$); (*d*) Mt/PPy ($R = 1/4$); (*e*) PPy.

14 Å for the PPy/Mt ($R = 0.25$) sample and it ranged from 13.1 to 13.4 A° for R within 0.5–4. Taking into account the thickness of the silicate layer (9.6 Å), an interlayer expansion of 4.2 Å was obtained for PPy/Mt ($R = 0.25$). However for nanocomposites with R within 0.5–4, the interlayer expansion is about 3.3–3.7 Å.

Comparing the values in Table 2 with those obtained in [5, 31–34], it can be specified that the intercalation of PPy in the clay causes an expansion of the clay interlayer of about 4.6 to 6.4 Å depending on the process and on the clay treatment. Thus, it can be concluded that these expansions are in accordance with the results obtained for the PPy/Mt (0.25) sample proving the success of a reaction of polymerization in situ of py and the formation of a PPy clay intercalated nanocomposite in this case. However, for R within 0.5–4, the expansion is slightly different, which presupposes that the structures in this case are different. It is well known that the morphology of PPy formed in Mt/PPy nanocomposites depends on both rate of polymerization of py and the sequence of py monomer diffusion. As mentioned above, although py monomers have been intercalated in the clay gallery, it was shown that the expansion of 3 nm did not correspond to a PPy ring; thus polymerization has occurred outside the clay interlayer, which proves that there are other factors involved in the in situ polymerization reaction [17]. As reported by Letaief and colleagues [17], the py polymerization kinetics is higher than the intercalation reaction thus giving rise to micro-composites instead of nanocomposites. In this way, PPy was formed around Mt tactoids and it coated the Mt surface rather than was inserted into Mt interlayers. To ensure the formation of an intercalated structure, Pourabbas and Peighambardoust [35] have exchanged the clay with interlayer Fe^{3+} cations as oxidant, thus ensuring the oxidant to be localized in the clay gallery,

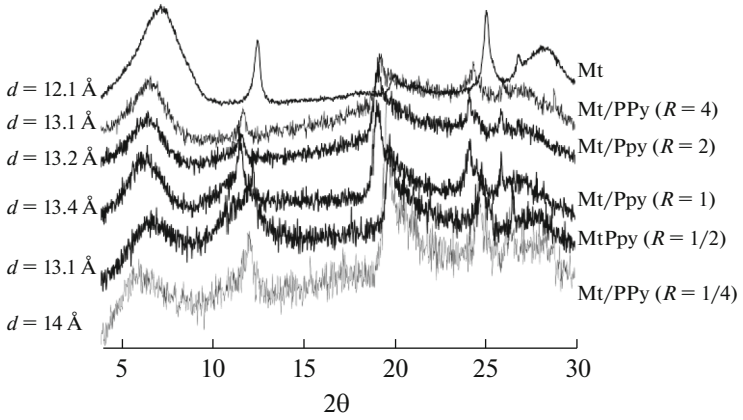

Fig. 4. XRD of Mt and Mt/PPy for: $R = 1/4$; $R = 1/2$; $R = 1$; $R = 2$; $R = 4$.

Fig. 5. Main types of intercalated nanocomposite.

so the in situ polymerization takes place only when py is diffused into the Mt interlayer where Fe^{3+} is present. The d_{001} obtained in this case was 1.5 nm compared to values reported in literature and corresponding to a monolayer of a PPy ring [31–34]. In all these studies, a step of organophilation of the clay with quaternary alkylammonium, or thermal or ultrasonic activation are necessary to form an intercalated nanocomposite.

Table 2. The d_{001} basal spacing cited in literature for different PPy-clay nanocomposites

Nanocomposites	Interlayer distance after polymerization, Å	References
PPy/Mt	16.65	[31]
PPy/Mt	16	[5]
Cu(I)–PPy/Mt	16.10	[32]
[Cu(I)–PPy/Clay]	16	[33]
PPy/Mt	14.24	[34]

However, sodium Mt without modification has been used; the idea was to vary the ratio of a monomer and an oxidant. Thus it has been proved that for a low amount of APS the in situ polymerization is possible. On the other hand, the obtained expansion approaches that of a montmorillonite exchanged with ammonium cations together with water molecules gives rise to d_{001} of about 1.2 nm [36]. Depending on R values, the morphology of PPy/clay nanocomposite is shown in Fig. 5.

The SEM micrographs in Fig. 6 demonstrate that Mt exhibited flaky aggregates, while pure PPy showed globular particles with a diameter of 400–600 nm. These types of morphologies of Mt and pure PPy are common in previous publications [20, 37, 38]. On the contrary, the Mt/PPy nanocomposites (Fig. 6) had a completely different morphology compared with that of a pure PPy. An obvious flake-like morphology was observed in the Mt/PPy nanocomposite micrographs, and these flake sheets became much looser and more separated with respect to Mt.

The EDX analysis of nanocomposite Mt/PPy (Fig. 7) shows the appearance of carbon, which proves

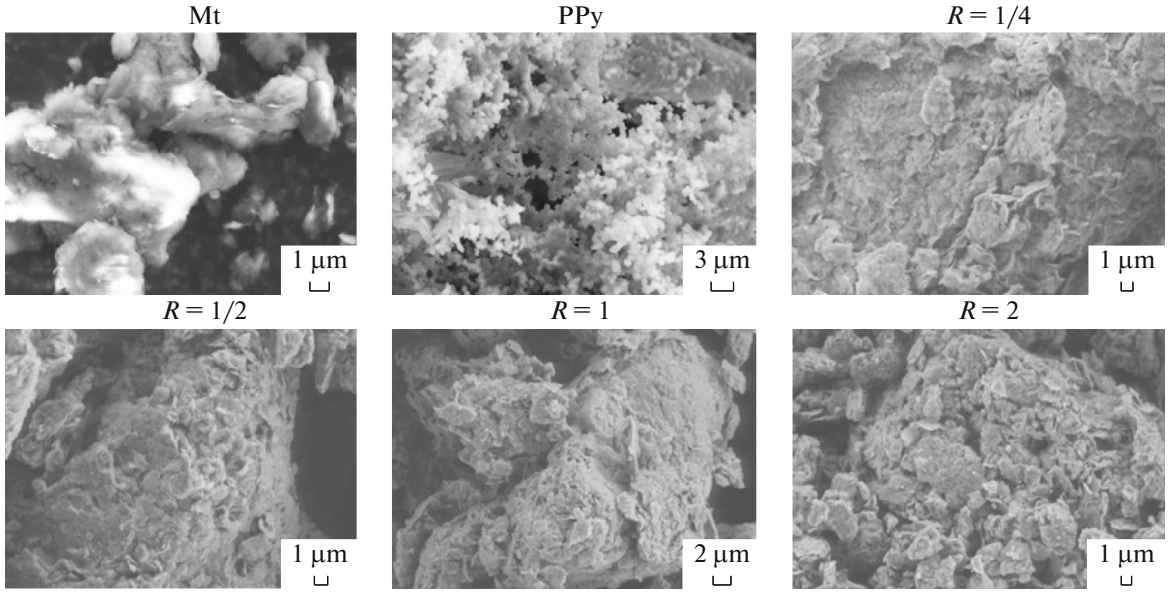

Fig. 6. SEM micrographs for Mt, for Mt, PPy/Mt ($R = 1/4$); PPy/Mt ($R = 1/2$); PPy/Mt ($R = 1$); PPy/Mt ($R = 2$) and PPy.

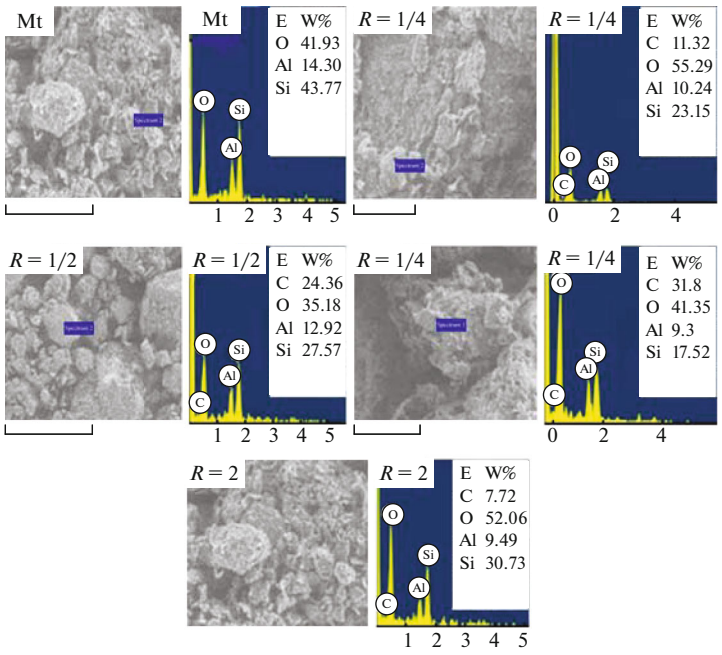

Fig. 7. EDX analysis of Mt, PPy/Mt ($R = 1/4$); PPy/Mt ($R = 1/2$); PPy/Mt ($R = 1$); PPy/Mt ($R = 2$); PPy/Mt ($R = 4$).

the py polymerization. A higher value of the carbon proportion (31.8%) is obtained for R corresponding to 1, which is in accordance with the obtained rate of polymerization. As shown above (Scheme 1), in theory, a molar APS/py ratio equal to 1 is required for a complete oxidation of py to a fully doped polymeric form.

Table 3 reports the specific surface area and micro-mesopore volume of Na-Mt. It can be seen the values decreased dramatically to 48 $m^2\ g^{-1}$ and 0.093 $cm^3\ g^{-1}$ for PPy/Na-Mt, respectively. This could be explained in terms of covering or filling of the pores by PPy [37–39].

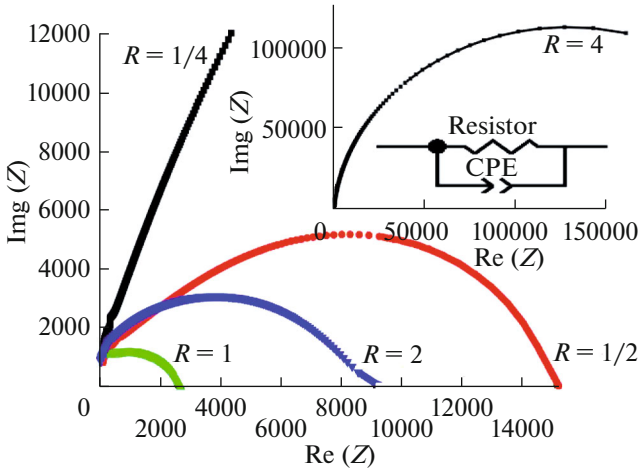

Fig. 8. The equivalent circuit and the Nyquist plots of: PPy/Mt (R = 1/4); PPy/Mt (R = 1/2); PPy/Mt (R = 1); PPy/Mt (R = 2); PPy/Mt (R = 4).

Mt composite was studied by plotting Z' against Z'' (Fig. 8), which depicts part of a semicircular arc. Ideally, in the case of the impedance of the bulk solid electrolyte, Nyquist's diagram is a semicircle with an equivalent circuit consisting of a resistance and a capacitor in parallel. As this semicircle is most commonly depressed, it is better to replace the capacitor with a constant phase element (CPE). The equivalent circuit can be expressed by a parallel connection of an ohmic resistor R' and a CPE (Fig. 8). The resistor (R') and the conductivities for all the composite systems are estimated and presented in Table 4.

As shown in Fig. 8 and Table 4, the higher the APS content, the higher the conductivity, reaching a value of 2.1×10^{-3} S cm^{-1} for R corresponding to 1, then it reaches a plateau value after a threshold. It is well known that the conductivity of Mt/PPy nanocomposites depends on the molar ratio of the oxidant to monomer and the arrangement of polymer. The findings are consistent with earlier reports that a high oxidant concentration leads to a low conductivity in PPy [40] and the properties of the oxidant solution influences the conductivity of PPy. This result can be accounted for by the over oxidation of a PPy chain, which leads to a later degradation and decrease of conductivity.

Table 3. Specific surface areas and specific micro-mesopore volumes of the Mt and PPy/Na-Mt nanocomposites

Sample	S_{BET}, m^2/g	Pore volume, cm^3/g
Mt	78.02	0.143
Mt/PPy (R = 1/2)	69.88	0.111
Mt/PPy (R = 1)	48.97	0.093
Mt/PPy (R = 2)	69.88	0.116

CONCLUSIONS

In this study, a PPy clay nanocomposite has been synthesized by a conventional solution intercalation method using APS as oxidant. Two parameters: (i) the amount of py to the cation exchange capacity of the clay and (ii) the ratio of APS to the intercalated py have varied. It was decided to increase the amount of clay compared to py in order to avoid a spontaneous external polymerization outside the clay. It was shown, that depending on the monomer clay ratio, py is inserted into the interlayer space of the clay forming a monolayer arrangement. While varying the ratio of the oxidant to py monomers, two different structures were obtained: an intercalated nanocomposite material for a low value of APS and a conventional microcomposite material for a high amount of the oxidant. The obtained structures are explained in terms of the competition and de-intercalation of py by the excess of ammonium cations.

The values of conductivities obtained for clay/PPy nanocomposites show clearly that electrically insulating clay may be converted to an electrically conducting nanocomposite material simply by introducing electrically conducting polymers together with mobile ions into their layer spaces. The materials should find applications as battery materials.

Table 4. Resistor and current conductivity of PPy/Na-Mt nanocomposites

APS/monomer molar ratio (R)	1/4	1/2	1	2	4
Conductivities, $\times 10^{-3}$ S cm^{-1}	0.0911	0.611	2.1	0.912	0.0237
Resistor, Ohm	14×10^4	1.6×10^4	3250	8400	24.5×10^4

REFERENCES

1. Aldissi, M., *Intrinsically Conducting Polymers. An Emerging Technology*, Dordrecht: Kluwer, 1993.
2. Nalwa, H.S., *Handbook of Organic Conducting Molecules and Polymers*, Chichester: Wiley, 1997, vol. 2
3. Skotheim, T.A., Elsenbaumer, R.L., and Reynolds, J.R., *Handbook of Conducting Polymers*, New York: Marcel Dekker, 1998, pp. 881–920.
4. Han, Y., *Polym. Compos.*, 2009, vol. 30, no. 1, pp. 66–69.
5. Kim, J.W., Liu, F., Choi, H.J., Hong, S.H., et al., *Polymer*, 2003, vol. 44, pp. 289–293.
6. Ruckenstein, E. and Hong, L., *Synth. Met.*, 1994, vol. 66, pp. 249–256.
7. Liu, Y.C., Huang, J.M., Tsai, C.E., Chuang, T.C., et al., *Chem. Phys Lett.*, 2004, vol. 387, pp. 155–159.
8. Dall'Acqua, L., Tonin, C., Varesano, A., et al., *Synth. Met.*, 2006, vol. 156, pp. 379–386.
9. Bae, W.J., Kim, K.H., Joa, W.H., and Park, Y.H., *Polymer*, 2005, vol. 46, pp. 10085–10091.
10. Eckle, M. and Decher, G., *Nano Lett.*, 2001, vol. 1, pp. 45–49.
11. Gomez, R., *Adv. Mater.*, 2001, vol. 13, pp. 163–174.
12. Graces, J.M., Moll, D.J., Bicerano, J., Fibiger, R., et al., *Adv. Mater.*, 2000, vol. 12, pp. 1835–1839.
13. Lin, J., Tang, Q., Wu, J., and Sun, H., *J. Appl. Polym. Sci.*, 2008, vol. 110, pp. 2862–2866.
14. Biswas, M. and Ray, S.S., *Mater. Res. Bull.*, 1999, vol. 34, pp. 1187–1194.
15. Mravcakova, M., Boukerma, K., Omastova, M., and Chehimi, M.M., *Mater. Sci. Eng. C: Mater. Biol. Appl.*, 2006, vol. 26, nos. 2–3, pp. 306–313.
16. Gao, I.W., Li, G., Yao, Y.F., and Jiang, J.M., *J. Macromol. Sci., Part B: Phys.*, 2011, vol. 50, pp. 1364–1375.
17. Letaief, S., Aranda, P., and Ruiz-Hitzky, E., *Appl. Clay Sci.*, 2005, vol. 28, pp. 183–198.
18. Faguy, P.W., Lucas, R.A., and Ma, W., *Colloid Surf. A*, 1995, vol. 105, no. 1, pp. 105–112.
19. van Olphen, H., *An Introduction to Clay Colloid Chemistry*, New York: Interscience, 1963, pp. 239–243.
20. Vaia, R.A. and Krishnamoorti, R., *Polymer Nanocomposites: Introduction. Polymer Nanocomposites Synthesis*, Washington, DC: Am. Chem. Soc., 2002.
21. Kuila, B.K. and Nandi, A.K., *Macromolecules*, 2004, vol. 37, pp. 8577–8584.
22. Tian, B. and Zerbi, G., *J. Chem. Phys.*, 1990, vol. 92, pp. 3892–3898.
23. Furakawa, Y., Tazawa, S., Fuji, Y., and Harada, I., *Synth. Met.*, 1988, vol. 24, pp. 329–341.
24. Tian, B. and Zerbi, G., *J. Chem. Phys.*, 1990, vol. 92, pp. 3886–3891.
25. Liu, J. and Wan, M., *J. Mater. Chem.*, 2001, vol. 11, pp. 404–407.
26. Ford, W.K., Duke, C.B., and Salaneck, W.R., *J. Chem. Phys.*, 1982, vol. 77, p. 5030.
27. Mellier, A., *J. Phys.*, 1967, vol. 29, p. 501.
28. Yoshimoto, S., Ohashi, F., and Kameyama, T., *Macromol. Rapid Comm.*, 2005, vol. 26, pp. 461–466.
29. Bredas, J.L., *Mol. Cryst. Liq. Cryst.*, 1985, vol. 118, pp. 49–56.
30. Wang, T., Liu, W., Tian, J., and Shao, X., *Polym. Compos.*, 2004, vol. 25, pp. 111–117.
31. Anuar, K., Murali, S., Fariz, A., and Ekramul, H.N.M., *Mater. Sci.-Medziagotyra*, 2004, vol. 10, no. 3, pp. 255–258.
32. Krishantha, D.M.M., Rajapakse, R.M.G., Tennakoon, D.T.B., and Dias, H.V.R., *J. Compos. Mater.*, 2005, vol. 40, pp. 1009–1021.
33. Rajapakse, R.M.G., Rajapakse, R.M.M.Y., Bandara, H.M.N., and Karunarathne, B.S.B., *Electrochim. Acta*, 2008, vol. 53, pp. 2946–2952.
34. Zahra Rizvi, T. and Shakoor, A., *J. Phys. D: Appl. Phys.*, 2009, vol. 42, pp. 095415–095421.
35. Pourabbas, B. and Peighambardoust, S.J., *Macromol. Symp.*, 2007, vol. 247, pp. 99–109.
36. Gautier, M., *Interactions entre argile ammoniee et molecules organiques dans le contexte du stockage des dechets, PhD These*, Orléans: Univ. d'Orleans, 2008.
37. Morgan, A.B. and Gilman, J.W., *J. Appl. Polym. Sci.*, 2003, vol. 87, pp. 1329–1338.
38. Yeh, J.M., Chin, Ch.P., and Chang, S., *J. Appl. Polym. Sci.*, 2005, vol. 88, pp. 3264–3272.
39. Chehimi, M.M., Boukerma, K., and Piquemal, J.Y., *Polymer*, 2006, vol. 47, pp. 569–576.
40. Hsu, C.F., Zhang, L., Peng, H., Travas-Sejdic, J., and Kilmartin, P.A., *Synth. Met.*, 2008, vol. 158, pp. 946–952.